Eur. Phys. J. E **11**, 255–271 (2003)
DOI 10.1140/epje/i2003-10019-5

THE EUROPEAN PHYSICAL JOURNAL E

Modelling thin-film dewetting on structured substrates and templates: Bifurcation analysis and numerical simulations

U. Thiele[1,a], L. Brusch[1], M. Bestehorn[2], and M. Bär[1]

[1] Max-Planck-Institut für Physik komplexer Systeme, Nöthnitzer Straße 38, D-01187 Dresden, Germany
[2] Lehrstuhl für Statistische Physik und Nichtlineare Dynamik, BTU-Cottbus, Erich-Weinert-Strasse 1, D-03046 Cottbus, Germany

Received 29 January 2003 and Received in final form 6 May 2003 /
Published online: 15 July 2003 –

Abstract. We study the dewetting process of a thin liquid film on a chemically patterned solid substrate (template) by means of a thin-film evolution equation incorporating a space-dependent disjoining pressure. Dewetting of a thin film on a homogeneous substrate leads to fluid patterns with a typical length scale, that increases monotonously in time (coarsening). Conditions are identified for the amplitude and periodicity of the heterogeneity that allow to transfer the template pattern onto the liquid structure ("pinning") emerging from the dewetting process. A bifurcation and stability analysis of the possible liquid ridge solutions on a periodically striped substrate reveal parameter ranges where pinning or coarsening ultimately prevail. We obtain an extended parameter range of multistability of the pinning and coarsening morphologies. In this regime, the selected pattern depends sensitively on the initial conditions and potential finite perturbations (noise) in the system as we illustrate with numerical integrations in time. Finally, we discuss the instability to transversal modes leading to a decay of the ridges into rows of drops and show that it may diminish the size of the parameter range where the pinning of the thin film to the template is successful.

PACS. 68.15.+e Liquid thin films – 81.16.Rf Nanoscale pattern formation – 47.20.Ky Nonlinearity (including bifurcation theory)

Thin liquid films on solid substrates often occur in nature and technology and have attracted many researchers [1]. They play important roles, for example, as liquid lining in mammalian lungs [2], as tear film in the eye [3], as protective, aesthetic, adhesive or lubricating coating, as functional layer in heat and mass transfer devices [4], or even in the form of lava or mud flow [5]. These liquid layers are characterised as thin because their thickness is small compared to typical length scales in the direction of the flow. This allows a simplification of the Navier-Stokes equations governing the free surface flow to a single nonlinear partial differential equation for the film thickness, a so-called film evolution equation [1]. Similar equations are also found for quite different physical problems. For instance, the dewetting of a thin film under the influence of effective molecular interactions [6–10] and the rupture of a thin liquid film on a heated horizontal plate [11–13] can be described by film evolution equations having a similar form as the Cahn-Hilliard equation known from the decomposition of a binary mixture [14]. The same is true for the respective problems on an inclined plane [11,13,15–17] and the driven Cahn-Hilliard equation [18]. Although the present work focuses on a specific system, namely, thin liquid films on inhomogeneous substrates, the main results will also apply to physically quite different situations.

Spontaneous dewetting occurs for liquid films with thicknesses smaller than one hundred nanometers where substrate-film interactions due to molecular forces become important. Thicker films may also dewet via heterogeneous nucleation. Up to now, most of the studies on dewetting focus on homogeneous substrates. All phases of the process are investigated: the initial rupture [19,20], the growth of individual holes [21,22], the evolution of the resulting hole pattern [22,23] and the stability of individual dewetting fronts [24]. The final goal is to understand how to keep thin films stable [25] or how to break thin films in a controlled manner [26].

This work addresses the study of the influence of chemically inhomogeneous substrates (templates) on the dewetting of a thin liquid film. Conditions for the heterogeneity that provoke dewetting at pre-determined points (pinning) will be obtained. Several experiments [27–32] involve dewetting processes of thin liquid films on heterogeneous substrates to deposit liquids in a regular manner determined by the template. In most experiments

[a] e-mail: thiele@mpipks-dresden.mpg.de

physically or/and chemically striped substrates are used. Reference [33] focuses on the phase ordering and dewetting of a binary mixture on hydrophobic and hydrophilic stripes, whereas in reference [27] the substrates are chemically striped and physically grooved. Pure dewetting without phase ordering is studied in references [30,31]. The surface (S) layer of a bacterium membrane can be used to deposit material in a controlled manner [34]. Beside these intentional heterogeneities, the substrate may also be heterogeneous due to impurities like oxidised patches, dust particles and scratches.

Previous theoretical results describe different morphological transitions of liquid layers on substrates with strong stepwise or nearly stepwise wettability contrasts [35–43]. The deposited liquid volume, chemical potential or the size of the heterogeneous patches have been used as control parameters. Earlier approaches involve diverging gradients of the chemical potential at the wettability steps [38,41].

Here, we study heterogeneous dewetting on a smoothly patterned substrate using the wettability contrast as a control parameter. Our results suggest, however, that the actual functional form of the heterogeneity is much less important than its length scale and its strength.

We employ bifurcation analysis using numerical continuation techniques [44] and illustrate the findings with simulations in time. Continuation is a very effective method to determine stable and unstable stationary solutions and their bifurcations by following them through parameter space using Newton's method [45,46]. For thin films continuation was applied recently in studies of dewetting on a homogeneous substrate [10,47,48], sliding drops on inclined planes [16,49], transversal front and back instabilities of sliding liquid ridges [50] and rivulet instabilities of a thin-film flow over a localized heater [51].

The transition from coarsening to pinning that occurs as the wettability contrast is increased was already subject of a short earlier study [52]. Here, we provide a more complete account by extending the bifurcation diagram to large system sizes. Furthermore, the transversal instability of striped liquid patterns is analysed in great detail and numerical simulations in interesting regions of the bifurcation diagram are carried out also with addition of noise to account for small random perturbations of the system.

We use an evolution equation for the film thickness [1] that includes a disjoining pressure to account for the effective molecular interaction between substrate and film. This approach can be used over a large range of length scales for the heterogeneities to investigate not only the equilibrium configurations but also the dynamics of the dewetting process on the structured surfaces. In particular, the dynamics cannot be predicted from the well-established approach based on variations of the interfacial free energy [35–37,42,43,53]. However, as a trade-off the thin-film equation is restricted to relatively small contact angles due to the use of the lubrication approximation in its derivation.

Depending on the particular problem treated, the disjoining pressure may incorporate long-range van der Waals and/or various types of short-range interaction terms [54–56]. These interactions are responsible for the process of dewetting. Studies of dewetting of a thin liquid film on a substrate are generally based on models involving a disjoining pressure [6–10,47]. A heterogeneous substrate may be modelled by a spatial variation of the disjoining pressure [38,41]. Recently, Pismen and Pomeau [57] derived a disjoining pressure that remains finite even for vanishing film thickness by combining the long-wave approximation for thin films [1] with a description for the diffuse liquid-gas interface [58]. These authors discuss the resulting vertical density profile near a horizontal liquid-gas interface. The density variation close to the solid substrate due to molecular interactions enters into their calculation via the boundary condition for the fluid density at the substrate. The obtained density profile is then incorporated into a fully consistent theory based on the Stokes equation in the long-wave approximation. The resulting film thickness equation has the usual form of a thin-film equation with a disjoining pressure [1]. The disjoining pressure is purely hydrodynamic in origin and its form is derived self-consistently rather than modelled. Pattern formation in this model was studied both for a liquid film on a homogeneous horizontal substrate [10,48] and for a film flowing down a slightly inclined plane [16]. Recent three-dimensional studies of sliding drops and liquid ridges on an inclined plane [17,49,50] revealed transverse instabilities.

The various results available for this model motivated us to employ it in the present study. A chemically striped substrate is modelled by a periodically modulated disjoining pressure. However, the main results for this model will not qualitatively differ from results for other disjoining pressures combining a short-range destabilising and a long-range stabilising component as, for example, used in [7,59–61]. This has been shown for homogeneous substrates in references [10,47,48].

Our study is organised as follows. In Section 1, we introduce the evolution equation for the film thickness, discuss the form of the disjoining pressure used, and nondimensionalise the equations. In Section 2, we determine stationary solutions and their linear stability properties. A morphological stability diagram is derived detailing parameter ranges for success or failure of templating.

In Section 3, these results are illustrated by and compared to (two-dimensional) numerical simulations in the parameter range of multistability. Section 4 gives the results for the transverse stability of the liquid ridges in dependence of the heterogeneity. Conclusions are drawn in Section 5.

1 Film thickness equation

The film thickness evolution equation for a very thin liquid film on a solid substrate is derived from the Stokes equations [1] using a long-wave or lubrication approximation. For a two-dimensional geometry, as sketched in Figure 1, one finds the evolution equation for the space- and

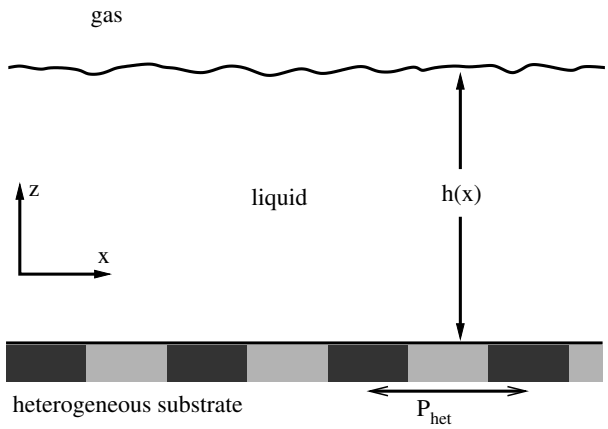

Fig. 1. Sketch of the two-dimensional geometry. The differently shaded regions of the substrate stand for the different wettability in the heterogeneous case.

time-dependent film thickness $h(x,t)$ on a homogeneous substrate as [10]

$$\partial_t h \;=\; -\nabla\,\left\{Q(h)\,\nabla\left[\gamma\Delta h - \partial_h f(h)\right]\right\}, \qquad (1)$$

where $Q(h) = h^3/3\eta$ is the mobility factor arising for Poiseuille flow. The term $\gamma\partial_{xx}h$ represents the Laplace or curvature pressure and $\partial_h f(h)$ is an additional pressure term. γ and η are the surface tension and viscosity of the liquid. Subscripts t, x and h denote the corresponding partial derivatives.

The additional pressure comprises the hydrostatic pressure and the effective molecular interaction between substrate and thin liquid film, *i.e.* the disjoining pressure:

$$\begin{aligned}\partial_h f(h) \;&=\; \kappa M(h,a) + \rho g h \\ &=\; \frac{2\kappa}{a}\,e^{-h/l}\,\left(1-\frac{1}{a}\,e^{-h/l}\right) + \rho g h\,, \end{aligned} \qquad (2)$$

where g is the gravitational acceleration and ρ the density of the liquid. $\Pi(h) = -\kappa M(h,a)$ is the disjoining pressure arising from diffuse interface theory [57], κ has the dimension of a spreading coefficient per length, a is a small dimensionless positive parameter describing the wetting properties in the regime of partial wetting, l is the length scale of the diffuse interface and $\rho g h$ is the hydrostatic pressure.

The heterogeneous substrate, we are interested in, is modelled by a spatial sinusoidal modulation of the overall strength of the disjoining pressure in equations (1, 2)

$$\kappa = \kappa_0\xi(x) = \kappa_0(1+\epsilon\cos 2\pi x/P_{\rm het}), \qquad (3)$$

amounting to a smooth spatial variation in the wettability of the substrate. The heterogeneity is characterised by the amplitude, ϵ, and the imposed periodicity, $P_{\rm het}$. The more and less wettable regions of the substrate are thereby chosen to have identical spatial size which provided successful templating at strong heterogeneities [41]. The maxima and minima of ξ represent the least and most wettable parts, respectively. We introduce dimensionless quantities (with tilde) using new scales:

$$\begin{aligned} t &= \frac{3\eta\gamma}{\kappa_0^2 l}\,\tilde t\,, \\ h &= l\,\tilde h\,, \\ x &= \sqrt{\frac{l\gamma}{\kappa_0}}\,\tilde x\,, \\ y &= \sqrt{\frac{l\gamma}{\kappa_0}}\,\tilde y\,. \end{aligned} \qquad (4)$$

The ratio $\kappa_0 l/\gamma$ is $O(a^2)$ [57], *i.e.* the scale in x-direction is $O(l/a)$. Equation (1) becomes, after dropping the tildes,

$$\partial_t h \;=\; -\nabla\,\left\{h^3\,\nabla\left[\Delta h - \xi(x)M(h,a) - Gh\right]\right\}, \qquad (5)$$

where

$$G = \frac{l\rho g}{\kappa_0} \qquad (6)$$

stands for the ratio of gravitation and molecular interactions. Its value is taken to be always positive. It was found that even a very small G cannot be dropped because the qualitative behaviour of the solution changes setting $G = 0$ [10,48]. However, because the actual value of $G < 1/4$ does not change the qualitative outcome, we use here a fixed $G = 0.1$.

The form of $M(h,a)$ allows to transfer the constant a into the mobility factor Q by introducing the shifted film thickness $h^\star = h + \ln a$. This allows to represent the stationary solutions independent of a and direct comparison with results for homogeneous substrate [10,48]. After dropping the star we find

$$M(h) \;=\; 2\,e^{-h}\,\left(1-e^{-h}\right), \qquad (7)$$

while the evolution equation (1) becomes

$$\partial_t h \;=\; -\nabla\,\left\{Q(h,a)\,\nabla\left[\Delta h - \partial_h f(h,x)\right]\right\} \qquad (8)$$

with $Q(h,a) = (h-\ln a)^3$, $\partial_h f(h,x) \;=\; \xi(x)M(h) + Gh$ and $\xi(x) = 1+\epsilon\cos 2\pi x/P_{\rm het}$.

The problem on the horizontal substrate has a variational structure. In consequence, one can give a Lyapunov function (free-energy potential) [6,10,11,62]

$$E(h) = \frac{1}{L^2}\int_0^L\int_0^L \left[\frac{1}{2}\nabla h\cdot\nabla h + f(h,x)\right]\mathrm{d}x\mathrm{d}y - f_0 \qquad (9)$$

that fulfills $\mathrm{d}E/\mathrm{d}t \le 0$. The normalising term f_0 denotes the free energy of the flat film of (scaled) thickness $\bar h$ on a homogeneous substrate ($\epsilon = 0$). We will call E shortly "energy" and use it to compare stationary solutions to determine their absolute stability. During the time evolution of a given initial film thickness profile, this energy decreases and eventually settles in a minimum when the system approaches a stationary solution of equation (8). Since the heterogeneity $\xi(x)$ is uniform in the y-direction, we analyse stationary solutions $h(x)$ that are uniform in y

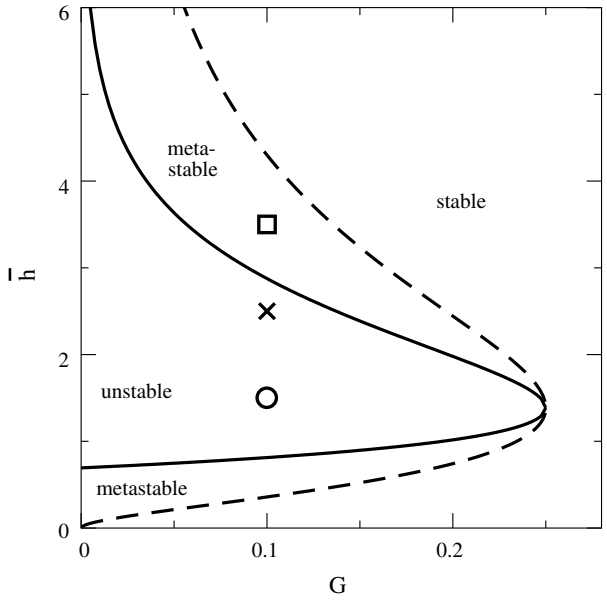

Fig. 2. The ranges for stable, metastable and linearly unstable flat films on the homogeneous substrate in the parameter plane $(G, \bar{h})$. The cross, square and circle indicate parameter values studied here in detail.

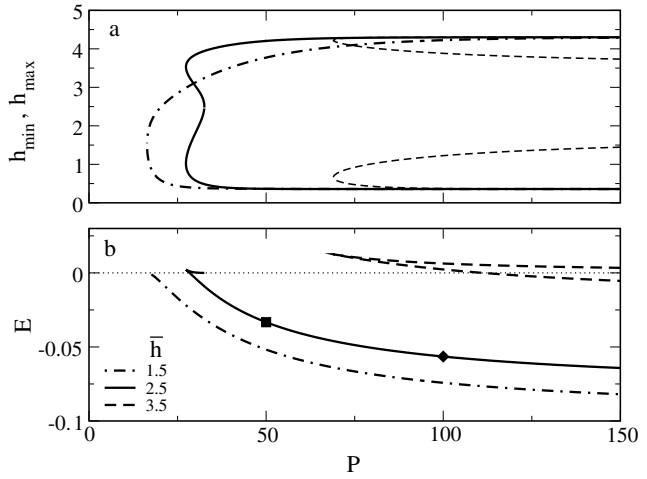

Fig. 3. Stationary periodic solutions on the homogeneous substrate. Shown are (a) the minimal and maximal film thicknesses and (b) the corresponding energies in dependence on the period for different mean film thicknesses as given in the legend and $G = 0.1$. Symbols denote solutions that are analyzed in detail (cf. Figs. 4 and 6, below).

as well. In contrast to the homogeneous case, these solutions are here of direct physical relevance. For strong heterogeneity they are the energetically favoured solutions even for the full three-dimensional problem. At weaker heterogeneity they may be stable or unstable with respect to three-dimensional disturbances as discussed in Section 4. However, simulations for striped substrates [41, 63] indicate that even in parameter ranges where the system approaches finally a solution depending on both x and y, the time evolution is first attracted by a stripe-like solution that subsequently decays into an arrangement of drops.

One can determine these stripe-like solutions directly by setting in equation (8) the time derivative and all y-derivatives to zero and integrating twice, yielding

$$0 = \partial_{xx} h - \xi(x) M(h) - Gh + C_1 \ . \tag{10}$$

The second integration is possible because the constant of the first integration can be set to zero. This is due to the fact that in the stationary states there is no mean flow in the system (corresponding to the variational structure). This is, for example, not the case for a drop on an inclined plate because there the structures are only stationary in a comoved frame [16]. Here we focus on situations with conserved liquid volume and use C_1 as a Lagrange multiplier to fulfill this volume constraint. Alternatively, C_1 corresponds to a chemical potential for situations with enabled evaporation.

2 Periodic solutions and their stability

2.1 The homogeneous substrate

Before considering the heterogeneous case, we will shortly review the results for the homogeneous case described by equation (8) with $\epsilon = 0$ [10,48]. Flat films are (trivial) stationary solutions that, depending on mean film thickness and the parameter G (see Fig. 2), may be unstable with respect to infinitely small (spinodal dewetting) or finite (nucleation) disturbances of the film surface. Rupture due to the spinodal mechanism occurs for disturbances with periods larger than a critical value $P_c = 2\pi/k_c$ with

$$k_c^2 = -\left.\frac{\partial M}{\partial h}\right|_{\bar{h}} - G, \tag{11}$$

whenever $\partial M/\partial h < -G$. The fastest growing wavelength is $P_m = \sqrt{2} P_c$.

Stationary solutions also exist as a continuous two-parameter family of periodic patterns, *i.e.* sequences of holes and droplets, parameterised by the mean film thickness $\bar{h} = 1/P \int_{x_0}^{x_0+P} h(x) \mathrm{d}x$ and the spatial period P of the pattern. Starting from small-amplitude sinusoidal solutions these branches are calculated using continuation techniques [44] as described in [10,16,50]. Details on the technique can be found in the first section of Appendix A. Three qualitatively different regimes exist as shown in Figure 3:

i) The mean film thickness corresponds to a linearly unstable flat film. One branch of stationary structured solutions exists whose amplitude (energy) increases (decreases) monotonically with increasing period. The energy (Eq. (9)) is always lower than the energy of the respective flat film. This case is illustrated by the dot-dashed curves in Figure 3.

ii) The mean film thickness also corresponds to a linearly unstable flat film. Two branches of stationary solutions exist. Their respective energies decrease monotonically with increasing period. The branch with lower energy corresponds to the branch found in i) but has now for a small range of periods an energy larger than the flat film. Its amplitude, however, still increases monotonically with increasing period. The other branch has always higher energy than the flat film, its amplitude decreases with increasing period and it terminates with small-amplitude solutions at the critical wavelength of the flat film P_c. It represents linearly unstable nucleation solutions that have to be overcome to break the film into small droplets with width smaller than P_c [10, 48]. In Figure 3 the solid curves illustrate this case.

iii) The mean film thickness corresponds to a metastable flat film. There exist two branches of stationary solutions much as in ii). However, because the flat film is linearly stable now also the branch of nucleation solutions continues towards infinite period. The nucleation solution at infinite period represents the individual critical hole necessary to break an infinitely extended film at a single site as discussed in [64] for first-order wetting transitions. The dashed curves in Figure 3 correspond to this case.

If dewetting proceeds via spinodal rupture of the film first holes with a typical distance, P_m, are formed as the solutions of the lower branch are approached. On a slower time scale the so formed initial drops coalesce, the pattern coarses and tends to the absolute minimum of the energy at the largest possible P, *i.e.* the system size. This often undesired coarsening may be stopped at an intermediate stage by evaporation of the solvent or by literally freezing the system [65,66]. The chemical structuring of the substrate, studied in the next section, opens a third way.

2.2 The heterogeneous substrate

We study the influence of the heterogeneity equation (3) by fixing the mean film thickness $\bar{h}$ and the parameter G in the linearly unstable film thickness range as indicated by the cross in Figure 2. Then the strength $\epsilon \geq 0$ and the period $P_{\rm het}$ of the heterogeneity are varied. The case $\epsilon < 0$ is related by symmetry. The system size is chosen as multiple of $P_{\rm het}$, $L = nP_{\rm het}$, and periodic boundary conditions are used. We will subsequently increase $n = 1, 2, 4, \ldots$ which allows to systematically construct the set of solutions and to understand their properties for a given system size.

Now, suppose a variety of substrates with fixed period $P_{\rm het}$ but different strength ϵ of the heterogeneity are available and a dewetting pattern with spatial period $P = P_{\rm het}$ is desired. One may first choose the mean film thickness $\bar{h}$ such that the critical wavelength of spinodal dewetting P_c is of the same order as $P_{\rm het}$. $P_{\rm het} = \sqrt{2}P_c$ warrants good templating for strong heterogeneity [41]. In the simplest case, the homogeneous system has only two stationary solutions with $P = P_{\rm het}$: the linearly unstable flat film and

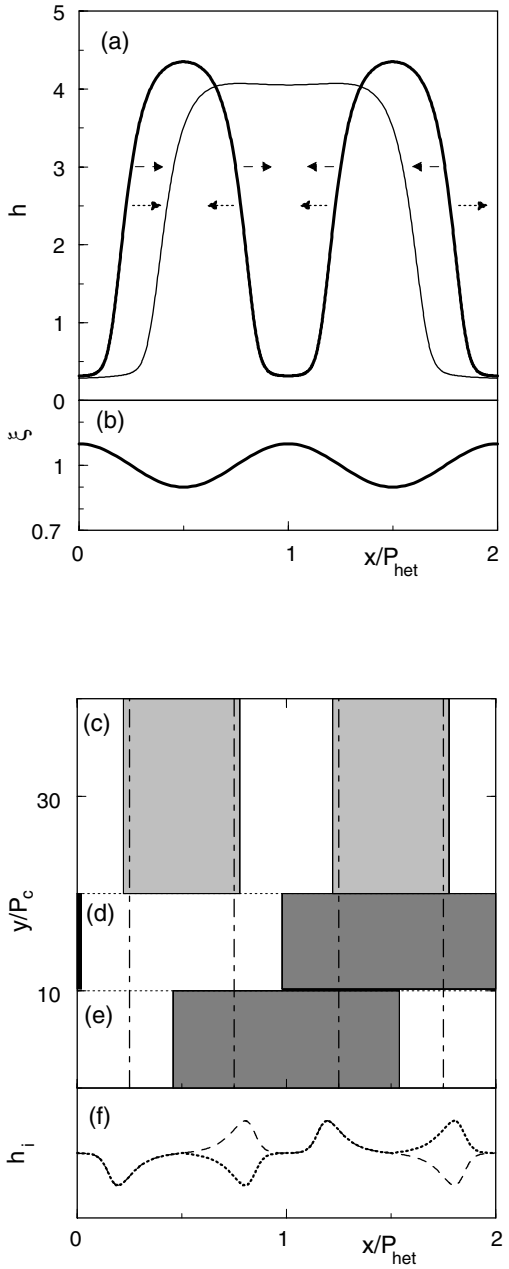

Fig. 4. Schematic overview of the two different longitudinal instability modes. (a) Profiles of stationary solutions to the film thickness equation (8) with spatial periods $P = P_{\rm het}$ (heavy line) and $P = 2P_{\rm het}$ (thin line) corresponding to the square and diamond in Figure 3, respectively. The dotted (dashed) arrows indicate the front movements for coarsening via the volume (translation) mode. (b) The heterogeneity $\xi(x)$ (Eq. (3)) for a chemically structured substrate. Minima of ξ correspond to the most wettable parts of the substrate. (c) Top view of the pinned solution $P = P_{\rm het}$. The liquid (indicated shaded areas) is collected on top of the more wettable stripes (indicated by vertical lines). This solution can coarse in two ways: (d) by mass transfer from the left to the right droplet (mediated by the dotted mode in (f)) or (e) by translation of both droplets (corresponding to the dashed mode in (f)). (f) The two linear eigenmodes of the pinned solution corresponding to the arrows of identical line styles in (a).

a periodic large-amplitude solution [10]. In Figure 3 the square corresponds to this pinned pattern if $P_{\rm het} = 50$. However, all stationary solutions with larger period have lower energy. The representative of these coarsed solutions with smallest period, *i.e.* $P = 2P_{\rm het}$, is marked by a diamond in Figure 3. The spatial profiles of the two competing solutions for a system of size $L = 2P_{\rm het}$ are shown in Figure 4 (a).

On the homogeneous substrate the wanted pattern is always linearly unstable to subsequent coarsening that transforms adjacent small droplets into a larger drop [10]. The coarsening takes one of two possible routes: i) translation of the drops towards each other as indicated by the upper line of arrows in Figure 4 (a), or ii) mass transfer from one drop to the other without translation as indicated by the lower line of arrows. The eigenmodes for these two routes are shown in Figure 4 (f). They are calculated via linear stability analysis of the periodic solutions (see App. A). The different coarsening modes were first discussed in the context of spinodal decomposition of a binary mixture [67].

Solutions with longer and longer periods result that have consecutively lower energies and the final state will always have a period equal to the system size. However, this intrinsic tendency towards coarsening enters now in competition with the heterogeneity (Fig. 4 (b)) that favors the solution with $P = P_{\rm het}$. For $L = 2P_{\rm het}$ this competition involves three solutions (Fig. 4 (c-e)) that can be stable or unstable depending on the parameters ϵ and $P_{\rm het}$.

2.2.1 System of size $L = P_{\rm het}$

We start our analysis in the smallest system $L = P_{\rm het}$. Switching on the heterogeneity implies, as a first consequence, that the flat film is no longer a solution of equation (10). The flat-film solution is replaced by a periodic solution that can be given analytically in the limit of weak heterogeneity $\epsilon \ll 1$. One writes the heterogeneity as $\epsilon\cos(kx) = \epsilon/2(e^{ikx} - \text{c.c.})$ with $k = 2\pi/P_{\rm het}$, where c.c. stands for complex conjugate. The volume conserving ansatz for the film thickness

$$h(x) = \bar{h} + \frac{\delta}{2}(e^{i\tilde{k}x} - \text{c.c.}) \qquad (12)$$

is inserted into equation (10) and gives for $\delta \sim O(\epsilon)$ and neglecting terms of higher order in ϵ solutions with $\tilde{k} = k$ and

$$\delta = \frac{M(\bar{h})}{k_{\rm c}^2 - k^2}\,\epsilon\,. \qquad (13)$$

The above-assumed condition $\delta \ll 1$ is only fulfilled if $P_{\rm het}$ is well separated from $P_{\rm c}$. $M(\bar{h})$ is always positive, hence for $k_{\rm c} > k$ ($P_{\rm c} < P_{\rm het}$) the solution is modulated in phase with the heterogeneity, *i.e.*, the film is thicker on the less wettable parts of the substrate. These small-amplitude solutions are linearly unstable like the flat film of the corresponding thickness without heterogeneity.

However, if the critical period is larger than the period of the heterogeneity ($P_{\rm c} > P_{\rm het}$), this solution has a phase shift of π with respect to the heterogeneity, *i.e.*, the film is thinner on the less wettable parts of the substrate. This is also the case if the flat film of thickness $\bar{h}$ is linearly stable because there $k_{\rm c}^2 < 0$. These small-amplitude solutions are linearly stable.

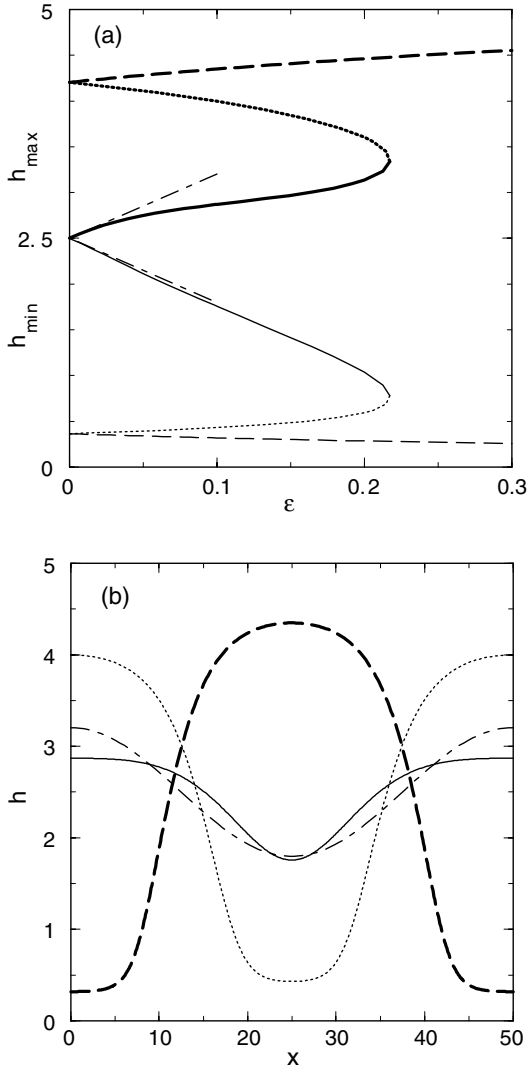

Fig. 5. (a) Bifurcation diagram representing maximal (heavy) and minimal (thin) film thickness of periodic stationary solutions. Line styles correspond to the ones of the profiles in (b). The small-amplitude result equation (13) is denoted by the dot-dashed lines. (b) Film thickness profiles of the solutions at $\epsilon = 0.1$. Parameters are $G = 0.1, \bar{h} = 2.5, P = P_{\rm het} = 50$ which yields $\delta/\epsilon = 0.7033$. The least and most wettable parts of the substrate are at $x = 0$ and $x = 25$, respectively.

Restricting ourselves again to linearly unstable mean film thicknesses we use the weakly modulated solution equations (12) and (13) as starting solution for the continuation procedure [44] (see App. A). As an example, we choose $G = 0.1$ and $\bar{h} = 2.5$ resulting in $P_{\rm c} = 33$, and use $P_{\rm het} = 50$. Then the stationary solutions with period $P = P_{\rm het}$ are computed as ϵ is increased. The flat-film and periodic solutions at $\epsilon = 0$ give rise to one and two solution branches, respectively. Figure 5 shows the

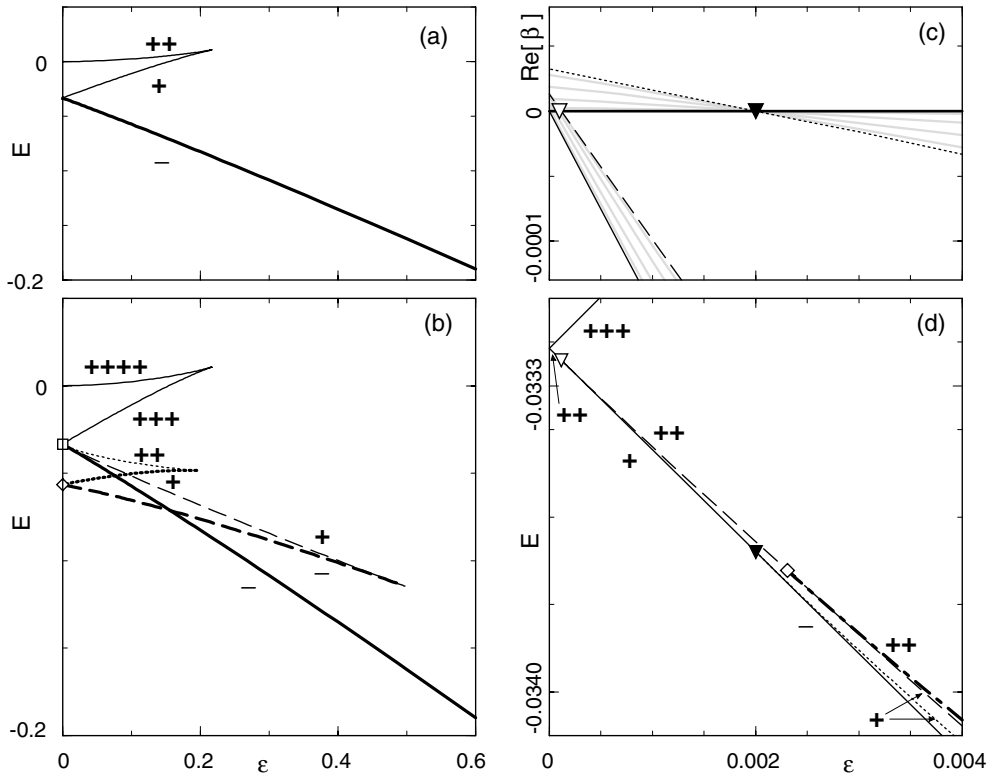

Fig. 6. Energy of stationary solutions to equation (8) with (a) $P = P_{\rm het}$ and (b) additional $P = 2P_{\rm het}$ *versus* ϵ. Square and diamond denote the solutions in the homogeneous case (Fig. 3). (c) Eigenvalues β with largest real part of the pinned pattern with $P = P_{\rm het}$ (lowest branch in (a)). Solid curves correspond to $L = P_{\rm het}$ and broken curves to $L = 2P_{\rm het}$. Triangles correspond to period doubling bifurcations in (d). Eigenvalues for $L = 10P_{\rm het}$ are denoted by gray lines. (d) Close-up of (b) using identical line styles. Solutions with $P = 2P_{\rm het}$ bifurcate from the branch with $P = P_{\rm het}$. Stable (unstable) solutions are marked by "–" ("+" for each unstable eigenmode). Parameters are $\bar{h} = 2.5$, $P_{\rm het} = 50$, $G = 0.1$ and $a = 0.1$.

corresponding bifurcation diagram and profiles of the solutions. The branch emerging from the flat-film solution is for small ϵ well approximated by the analytical result equation (13). The solutions on this branch are indeed in phase with the heterogeneity whereas the branch of lowest energy that corresponds to large-amplitude solutions possesses a phase shift, as one would expect from physical considerations: the drops concentrate on the more wettable patches. The middle branch is in phase with the heterogeneity and terminates in a saddle-node bifurcation with the small-amplitude branch.

In Figure 6(a) the relative energies of the solutions shown in Figure 5(a) are compared. For the chosen values of the parameters the solutions in phase have a larger energy than those out of phase. When increasing ϵ the energy of the lower branch decreases further whereas the energies of the other branches increase.

In a system that has the size of one period of the heterogeneity, *i.e.* $L = P_{\rm het}$, the entire lower branch in Figure 6(a) is linearly stable indicated by a "–" whereas the other two branches are linearly unstable indicated by "+" or "++" corresponding to the number of unstable eigenvalues. For $\epsilon = 0$ all solutions possess two zero eigenvalues (neutral modes) that correspond to the symmetries with respect to translation and change of mass. As ϵ departs from zero, the translational symmetry is broken and one of the two zero eigenvalues acquires a negative real part, shown for the stable branch as a thin solid line in Figure 6(c)). The second symmetry corresponds to a shift along the family of solutions with different $\bar{h}$ that are all solutions to the same equation (8). Since the heterogeneity does not destroy the possibility of this shift the second eigenvalue remains equal to zero (thick solid line in Fig. 6(c)).

New solutions appear as we increase the system size to $L = n\,P_{\rm het}$. Beside the already discussed solutions with period $P = P_{\rm het}$ there also solutions with period $P = iP_{\rm het}$ exist, where i and n/i are integers. For instance, in a system of size $L = 8P_{\rm het}$ beside the pinned solution with period $P = P_{\rm het}$ there appear solutions with $P = 2P_{\rm het}$, $4P_{\rm het}$ and $8P_{\rm het}$.

2.2.2 System of size $L = 2P_{\rm het}$

Next we consider the doubled system size $L = 2P_{\rm het}$. For this system solutions exist with two periods: i) $P = P_{\rm het}$ and ii) $P = 2P_{\rm het}$ as shown in Figure 6 (b). At $\epsilon = 0$ they are denoted by a square i) and a diamond ii) corresponding to the solutions in Figure 3. For increasing ϵ the solutions with $P = P_{\rm het}$ are the same as discussed above for the smaller system ($L = P_{\rm het}$). However, now the

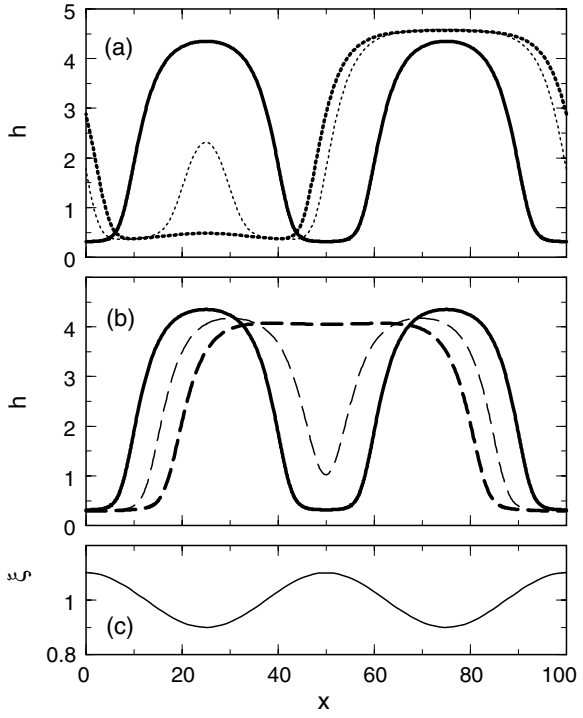

Fig. 7. Profiles for a system of size $L = 2P_{\rm het}$. The dotted and dashed lines denote solutions with $P = 2P_{\rm het}$ situated on the branches with corresponding line styles in Figure 6 (b). The solid lines show the pinned solution corresponding to the solid line of lowest energy in Figure 6 (b). Solutions drawn with broken lines in (a) and (b) can be obtained from the pinned solution by mass transfer and translation, respectively. Thereby, the solutions shown as thin lines take the role of a saddle between the respective other two solutions. Parameters are $\bar{h} = 2.5$, $P_{\rm het} = 50$, $\epsilon = 0.1$ and $G = 0.1$. The panel (c) shows the heterogeneity $\xi(x)$ with minima corresponding to the most wettable parts of the substrate.

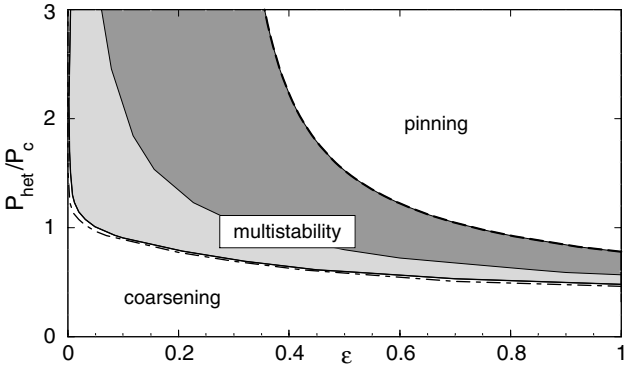

Fig. 8. Morphological phase diagram of templating shows parameter $(\epsilon, P_{\rm het}/P_{\rm c})$ regions with different behaviour of the thin film on a heterogeneous substrate. The shaded band separates the parameter region of coarsening from the one of pinning. Inside the shaded band multistability is present with the pinned pattern having the minimal energy inside the dark shaded area. The pinned solution is unstable to longitudinal perturbations ($k = 0$) below the dot-dashed curve and unstable to transversal perturbations ($k \neq 0$) below the shaded band (solid curve). Parameters are $\bar{h} = 2.5$ and $G = 0.1$.

stability analysis shows the appearance of two new eigenvalues (Fig. 6(c)) that correspond to asymmetric combinations of the neutral modes. They correspond to the two *different* modes of coarsening introduced above. i) The dashed line in Figure 6(c) belongs to a combination of opposite translational modes leading to droplet translation. ii) The dotted line belongs to a combination of opposite volume modes leading to mass transfer.

For the present choice of parameters, Figure 6(c) shows that the shift mode becomes stable at smaller ϵ values than the mass transfer mode. So the mass transfer is the dominant coarsening process. As ϵ increases, both eigenvalues become negative, implying the linear stability of the solution with $P = P_{\rm het}$ for larger ϵ. At the crossing points, two period doubling bifurcations (triangles) occur where stationary solutions of period $P = 2P_{\rm het}$ emerge (compare Fig. 6(c,d)). The two bifurcations are both subcritical, hence the emerging solutions inherit the respective instability of the unstable solutions at smaller ϵ [68].

Therefore, the four branches of solutions with $P = 2P_{\rm het}$ shown in Figure 6 (b) have the following linear stability. The upper dotted branch (see also profile in Fig. 7 (a)) carries two positive eigenvalues and is itself a saddle in function space that divides evolutions by mass transfer towards the lower dotted branch and the $P = P_{\rm het}$ branch. The lower dotted branch (profile in Fig. 7 (a)) still has one positive eigenvalue that leads to a shift of the pattern towards solutions of the lower dashed branch. The upper dashed branch (profile in Fig. 7 (b)) has one positive eigenvalue and is a saddle that divides evolutions by translation of two droplets towards the lower dashed branch and the $P = P_{\rm het}$ branch. The entire lower dashed branch (profile in Fig. 7 (b)) is linearly stable in $L = 2P_{\rm het}$ and represents the coarse solution competing with the desired pattern.

Comparing Figure 6 (b) and (d) we note that the numbers of unstable eigenvalues for the two bifurcating branches differ near and far from the period doubling bifurcations. This is due to two additional pitchfork bifurcations occurring at $\epsilon = 0.0022$ (diamond symbol, dashed branch) and $\epsilon = 0.04$ (dotted branch). The short dot-dashed branch stands actually for two branches of identical energy and consists of solutions with broken mirror symmetry. They connect the pitchfork bifurcations and transfer an unstable eigenvalue to the mass transfer branch (dotted). Although the additional solutions are all linearly unstable they may influence the coarsening dynamics in this ϵ range.

Summarising the results on the stability of the solutions in a system of size $L = 2P_{\rm het}$ at the given parameter values, one can state that for $\epsilon < 0.002$ solutions with $P = 2P_{\rm het}$ are the only stable ones and have lowest energy. For $\epsilon > 0.002$ multistability between solutions with $P = P_{\rm het}$ and $P = 2P_{\rm het}$ occurs and the initial condition becomes important for the dewetting of a thin film on a heterogeneous substrate. At $\epsilon = 0.157$ the energies of both solutions are equal. At larger ϵ the desired pattern has

lowest energy. If suitable initial conditions can be chosen, then the pinned solution can already be obtained at much smaller ϵ. However, as illustrated by simulations in time in Section 3, coarsening will still occur at much larger ϵ if disadvantageous initial conditions are chosen. The pinned solution is the only possible for $\epsilon > 0.5$, where the linearly stable $P = 2P_{\rm het}$ branch ceases to exist.

Up to now, we discussed the ϵ ranges for coarsening, multistability and pinning for a single choice of $P_{\rm het}$. We repeated the above analysis for the full range of $P_{\rm het}$ keeping $G = 0.1$ and $\bar{h} = 2.5$ fixed. The results are presented in the "morphological phase diagram", Figure 8. At low values of $\epsilon P_{\rm het}$ coarsening prevails while for large values the pattern is pinned to the heterogeneity. At intermediate values (shaded band) the initial condition selects the asymptotic state due to multistability. In particular, it is not possible to pin a pattern to a heterogeneity that is much smaller than the critical wavelength $P_{\rm c}$ for the surface instability of the corresponding flat film on the homogeneous substrate.

2.2.3 Large system size

In systems of larger size L, new combinations of the neutral modes lead to an increasing number of unstable eigenmodes for the pinned pattern. All new positive eigenvalues lie between those of $L = 2P_{\rm het}$, decrease with increasing ϵ and eventually become negative as shown in Figure 6 (c) for $L = 10P_{\rm het}$. Hence the coarsening instability is most dominant for nearest-neighbour interaction and is already covered by the analysis of the short system $L = 2P_{\rm het}$ [52]. So the pinned pattern in an arbitrarily large system is linearly stable against coarsening for heterogeneities $\epsilon > 0.002$. This critical ϵ is determined by the parameters $\bar{h}, G$ and the specific form of $\Pi(h)$. However, since the two symmetries connected with the coarsening modes are present for arbitrary choices of $\Pi(h)$ the result does not qualitatively depend on this choice.

Each zero crossing of one of these new eigenvalues corresponds to a bifurcation of a branch of coarsed solutions. This explains the massive proliferation of solutions in larger systems. To illustrate this, Figure 9 shows solutions with $P = 4P_{\rm het}$ in the bifurcation diagram for systems of size $L = 4P_{\rm het}$. Solutions with $P = 2P_{\rm het}$ and $P = P_{\rm het}$ have to be added according to Figure 6(b) and possess an internal discrete translational symmetry in $L = 4P_{\rm het}$. All solid branches in Figure 9 emerge at two period quadrupling bifurcations of the pinned solution $P = P_{\rm het}$. Both occur at $\epsilon \approx 0.002$ ($E \approx 0.0338$). Following the solutions along these branches (also through the saddle node bifurcations), smaller droplets continuously merge into larger ones as is illustrated in the inset for two solutions corresponding to the symbols in the main panel. At $\epsilon = 0 (E \approx 0.068)$ the branches connect and the solutions approach the single droplet of system size known from the homogeneous system. At finite ϵ, the coarse solutions possess small satellite drops beside the large drop. The latter may cover many stripes, but the small satellite drops prevail even at the end of a complete coarsening process.

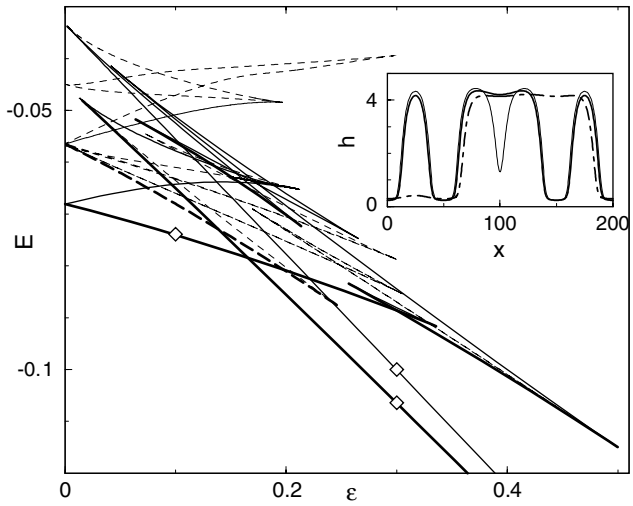

Fig. 9. Bifurcation diagram for $L = 4P_{\rm het}$, solutions with $P = 2P_{\rm het}$ and $P = P_{\rm het}$ are excluded. Thin (heavy) solid lines denote unstable (stable) solutions for $P = 4P_{\rm het}$ that emerge from the single droplet at $\epsilon = 0, E = -0.068$. Dashed curves are examples of branches that bifurcate from symmetrical solutions with $P = 2P_{\rm het}$ and $P = P_{\rm het}$ at small $\epsilon \approx 0.001$. The two lower branches exist up to $\epsilon = 1.17, E = -0.295$. The inset shows profiles corresponding to the diamonds with corresponding line styles for $\epsilon = 0.3$ and the dot-dashed line for $\epsilon = 0.1$. Parameters are $\bar{h} = 2.5$, $P_{\rm het} = 50$, $G = 0.1$ and $a = 0.1$.

We find 5-branch segments of linearly stable solutions and denote them by heavy lines. Four out of these 5 belong to the branches described above and can be easily computed when starting from the solution with a single large drop at $\epsilon = 0$. This procedure is robust and can be generalised to arbitrary system size. Practically, computer resources become demanding as the number of modes in the continuation procedure increases linearly with the system size. One out of the 5 stable segments belongs to a set of independent branches (denoted by dashed curves) that interconnect bifurcations of branches with $P > P_{\rm het}$. Most emerge and terminate at small but always finite ϵ. Note, especially, the two lines terminating in a saddle node at $\epsilon \approx 0$ and $E \approx 0.045$. They come close to but do not reach the solution with $P = 4P_{\rm het}/3$ that exists in the homogeneous system.

2.2.4 Changing the film thickness

We repeated the above analysis for systems of size $L = 2P_{\rm het}$ for different choices of the film thickness and concentrate here on the qualitative changes compared to $\bar{h} = 2.5$ studied above. In Figure 10 the bifurcation diagrams are shown for (a) the lower part of the linearly unstable range at $\bar{h} = 1.5$ choosing $P_{\rm het} \approx \sqrt{2}P_{\rm c}(\bar{h})$, and (b) in the metastable range at $\bar{h} = 3.5$, where $P_{\rm het} = 130$ was chosen. In the metastable range there exist three solutions with $P = P_{\rm het}$ in the homogeneous system. This results for $\epsilon \neq 0$ in one additional pair of solutions as compared to the linearly unstable thickness range. Solutions with $P = 2P_{\rm het}$ are similar to the case with $\bar{h} = 2.5$. The stable

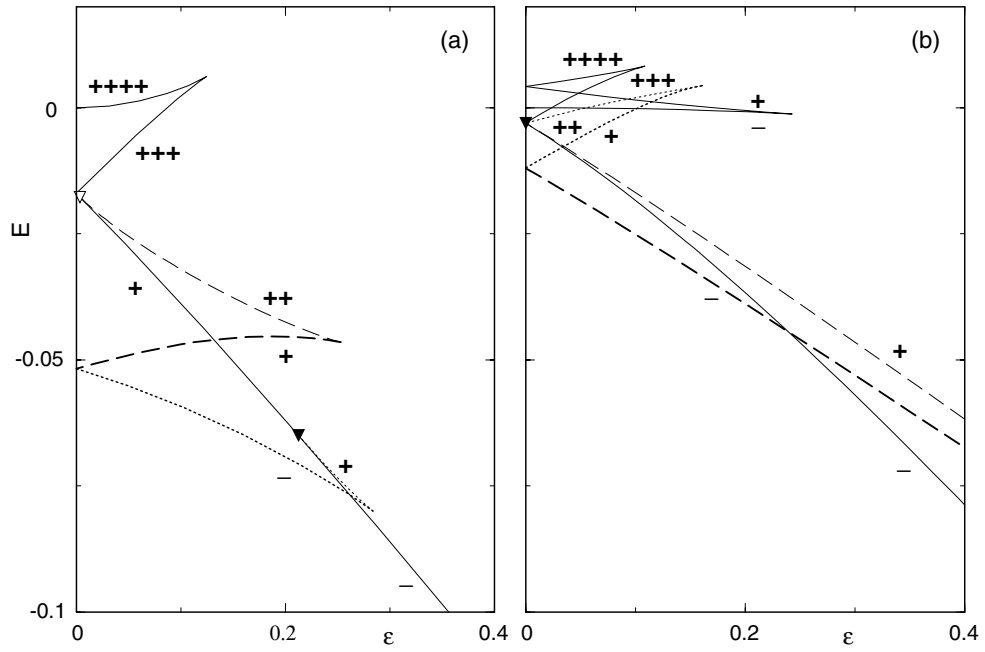

Fig. 10. Energy of stationary solutions $P = P_{\rm het}$ (solid curves) and $P = 2P_{\rm het}$ (broken curves) *versus* ϵ for (a) small film thickness $\bar{h} = 1.5$ (square in Fig. 2) and (b) large $\bar{h} = 3.5$ in the metastable range (circle in Fig. 2). Stable (unstable) solutions are marked by "−" ("+" for each unstable eigenmode). Triangles denote period doubling bifurcations where solutions with $P = 2P_{\rm het}$ emerge due to the translation mode (dashed branch, open triangle) and transfer mode (dotted branch, filled triangle), compare Figure 6. In (b) another pair of broken curves ($P = 2P_{\rm het}$) is omitted. This pair connects two period doubling bifurcations on the $P = P_{\rm het}$ branch maked with a single "+" and intersects the $\epsilon = 0$ axis at $E = 0.0017$. Parameters are $G = 0.1$ and (a) $P_{\rm het} = 25$, (b) $P_{\rm het} = 130$.

branch of coarse solutions also corresponds to the translation of droplets. Hence, for thick films $\bar{h} > \ln 4$, the stable coarse drop is always centered on a least wettable position and overlaps the adjacent more wettable areas.

For small film thickness $\bar{h} = 1.5$ (Fig. 10 (a)) the solutions with $P = P_{\rm het}$ are similar as for $\bar{h} = 2.5$, since there are also only two solutions in the homogeneous limit. However, although the sequence of the two bifurcations that stabilise the pinned solution is as for $\bar{h} = 2.5$, the branches with $P = 2P_{\rm het}$ exchange their role, *i.e.* the stable coarse solution is now generated by the transfer mode. The reason is that at small $\bar{h} < \ln 4$ the coarse drop $P = 2P_{\rm het}$ contains an amount of material small enough to benefit from completely covering a more wettable area and avoiding overlap with the less wettable areas. Therefore, the additional pitchfork bifurcations that are needed for larger thicknesses to transfer an eigenvalue between the two coarse branches are no longer present. Moreover, the stabilisation of the pinned solution with respect to coarsening due to volume transfer occurs at much larger $\epsilon \approx 0.21$ yielding only a narrow range of multistability. In summary, we find that the morphological phase diagram Figure 8 is qualitatively similar as for film thickness $\bar{h} > \ln 4$, but only shows a narrow band of multistability.

3 Time evolution

We have studied the stationary solutions and their bifurcation structure using the strength of the heterogeneity as control parameter. From this analysis we predict parameter ranges for pinning, coarsening and multistability (Fig. 8). In order to test these predictions and to illustrate the occurring processes we study here the evolution in time for some selected parameter values by numerically integrating equation (8) for different initial conditions. The details of the used numerical procedure are explained in Appendix A.

As a first example, Figure 11 shows the long-time evolution for a homogeneous system in comparison with a heterogeneous system where coarsening can still occur, *i.e.* with a very small heterogeneity. We show these evolutions under the influence of a very small additive noise to take into account the small perturbations of the systems that can nearly not be excluded on the long timescale of the coarsening process. However, we do not intent here to study systematically the influence of noise and will only note its effects in passing. Details with respect to the used noise are given in the last section of Appendix A. In Figure 12 the energy equation (9) is plotted in dependence of time for different realizations of the noise. The solid and dashed lines indicate the respective evolution without and with heterogeneity. The thin lines indicate the evolution without noise.

We note that the coarsening starts much earlier for the homogeneous system than in the heterogeneous case, corresponding to the result of the linear stability analysis (Fig. 6 (a)). However, the actual coarsening seems to advance faster for the slightly heterogeneous system.

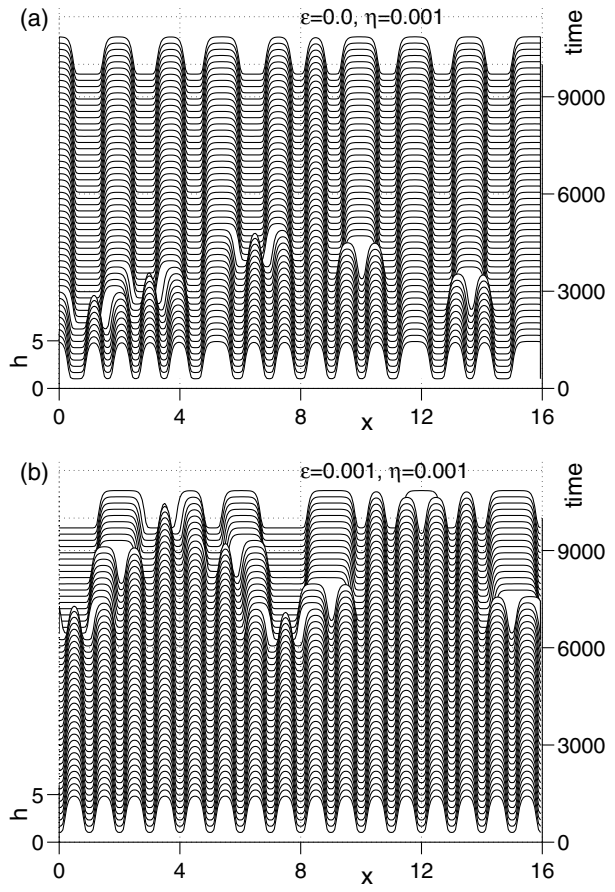

Fig. 11. Space-time plots showing the profiles for (a) homogeneous substrate ($\epsilon = 0.0$) and (b) slightly heterogeneous substrate ($\epsilon = 0.001$). The remaining parameters are $\bar{h} = 2.5$, $P_{\rm het} = 50$, $G = 0.1$ and $a = 0.1$. The initial condition is a flat film with a small dent in the center. A small noise of amplitude $\eta = 0.001$ is added. The coordinate x is plotted in units of $P_{\rm het}$.

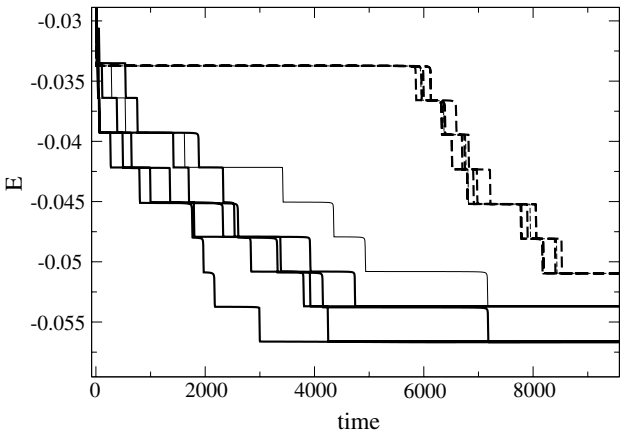

Fig. 12. Energy for the long-time evolution for the homogeneous substrate (solid lines) and a slightly heterogeneous substrate (dashed lines, $\epsilon = 0.001$). The thin lines represent the respective evolutions without noise. The different heavy lines stand for evolutions with different realizations of noise with $\eta = 0.001$. The remaining parameters are as in Figure 11.

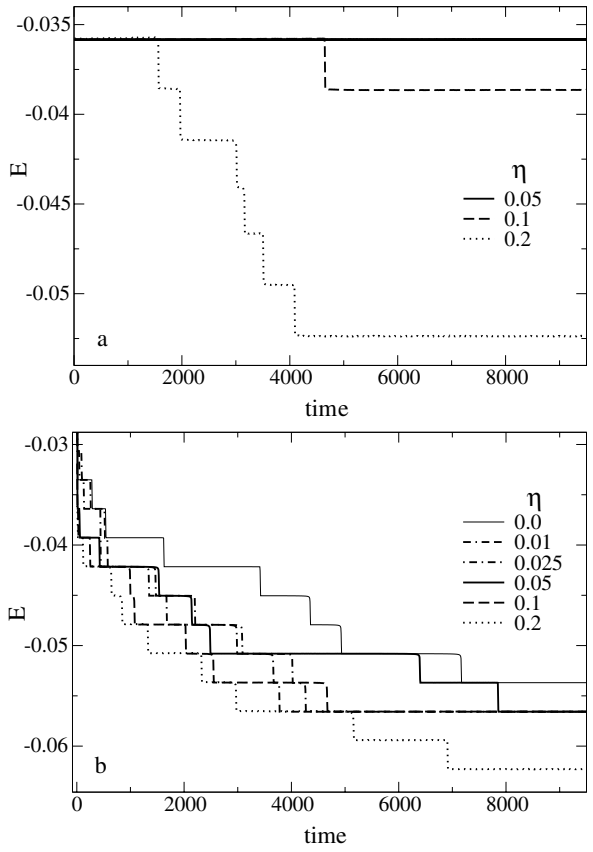

Fig. 13. Energy for the long-time evolution under the influence of noise of different strength (as given in the legends) for (a) a heterogeneous substrate with $\epsilon = 0.01$ and (b) a homogeneous substrate. The remaining parameters are $\bar{h} = 2.5$, $P_{\rm het} = 50$, $G = 0.1$ and $a = 0.1$.

Furthermore, for the heterogeneous system the small noise makes no difference when compared to the evolution without noise, whereas for the homogeneous system the evolution seems to be slightly slower without noise. This may indicate that the coarsening with heterogeneity is determined by the heterogeneity itself. In Figure 11 it can be clearly seen that the individual coarsening processes are initiated by mass transfer between the individual drops as was indicated by the linear stability analysis (Fig. 6 (c)). However, it is interesting to note that the local processes may involve two drops (the two local processes on the right side of Figure 11 (a)) or three drops (the three local processes on the left side of Fig. 11 (a)).

For a larger heterogeneity the pinned solution is linearly stable. Therefore, no coarsening occurs without the presence of additional influences. However, the system is in the multistable range, *i.e.* there exist also coarse solutions that are linearly stable and for a modest heterogeneity even have a lower energy than the pinned solution. Here we use two methods to illustrate the multistability. One way is to add noise to the system as already done above. Figure 13 (a) shows the energy in the course of the long-time evolution of a system with a heterogeneity already deep in the linearly stable range for the pinned solution

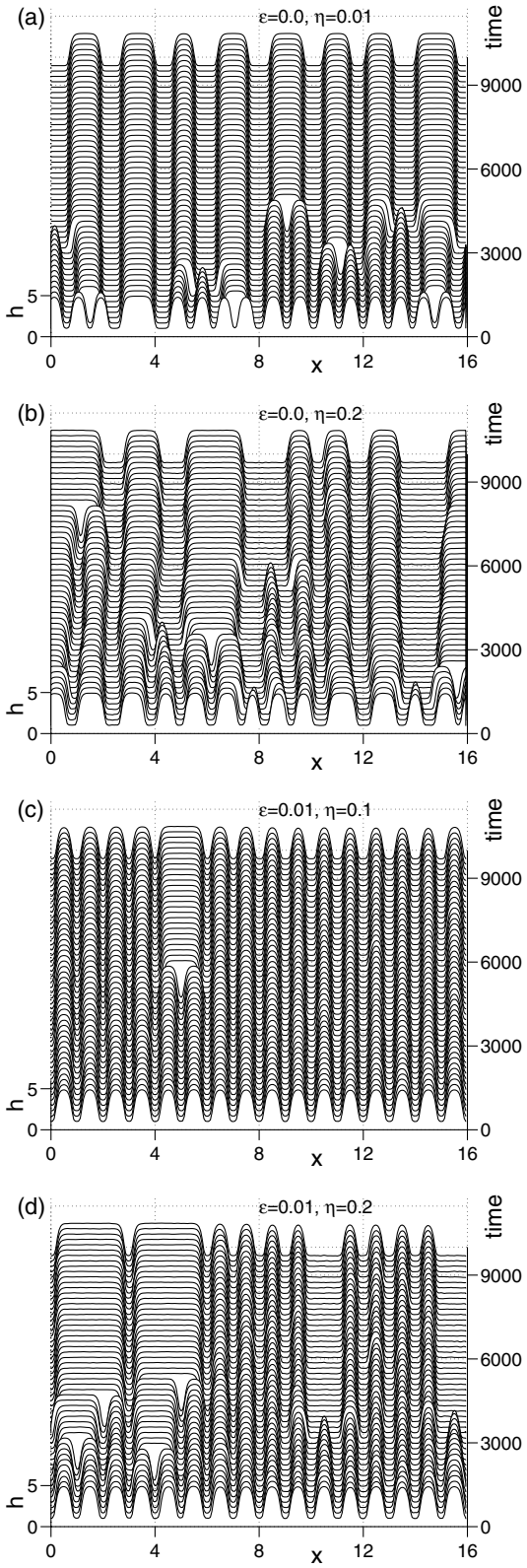

Fig. 14. Space-time plots illustrating the long-time evolution for different heterogeneity and noise strengths corresponding to selected curves of Figure 13. (a) $\epsilon = 0.0, \eta = 0.01$, (b) $\epsilon = 0.0, \eta = 0.2$, (c) $\epsilon = 0.01, \eta = 0.1$, and (d) $\epsilon = 0.01, \eta = 0.2$. The coordinate x is plotted in units of $P_{\rm het}$.

($\epsilon = 0.01$). One can see that a noise of a certain strength can bring the system from the local energy minimum of the pinned solution to the global minimum, or at least a lower minimum of some coarse solution. However, the process depends strongly on the noise. For comparison, we show in Figure 13 (b) the evolution of the homogeneous system for different noise strengths. There the noise slightly accelerates the coarsening, but the strength of the noise has little influence. Space-time plots are shown for both cases in Figure 14. Note that in the homogeneous case with very strong noise (Fig. 14 (b)) the local processes have now a clearly visible contribution from the translational mode. Another noteworthy effect occurs in the heterogeneous case with strong noise (Fig. 14 (d)). The coarsening does not proceed through local processes but rather through a global mode, *i.e.* material is transfered from one half of the system to the other. An indication for this process gives already the bifurcation analysis for the system of size $L = 4P_{\rm het}$ (Fig. 9), where it was shown that for ϵ not too large the solution with $P = L$ has a lower energy than the solution of period $P = 2P_{\rm het}$.

By adding noise we studied the consequence of the multistability for the long-time evolution. Multistability also affects the short-time evolution as can be seen using different initial conditions. Specifically, we start in a system of size $P = 4P_{\rm het}$ from a flat film with a sinusoidal modulation of amplitude $d \times \bar{h}$ and period $2P_{\rm het}$ to give a bias towards the coarse solution that spans two heterogeneity periods. In the homogeneous system even the very small $d = 0.005$ induces a skipping of the solution with period $P = P_{\rm het}$ in the time evolution: the system goes directly to the $P = 2P_{\rm het}$ solution as can be seen in Figure 15 (a), where the evolution of the energy is plotted for different amplitudes d. However, in the further course of the time evolution the system will take another coarsening step to the $P = 4P_{\rm het}$ solution.

In the heterogeneous system a stronger bias is necessary to favour the coarse solution. So in the multistable sub-range where the coarse solution has the lower energy ($\epsilon < 0.2$ for the used parameters) at $\epsilon = 0.01$ an amplitude $d \approx 0.05$ is sufficient whereas at $\epsilon = 0.1$ (Fig. 15 (b)) already $d \approx 0.17$ is needed to go directly to the coarse solution. In the multistable sub-range where the pinned solution has lower energy ($\epsilon > 0.2$ for the used parameters) it is still possible to obtain the coarse solution in the short-time evolution. However, a relatively strong bias is needed as shown in Figure 15 (c) for $\epsilon = 0.3$, where the necessary bias is $d \approx 0.37$, *i.e.* nearly 40% of the mean film thickness. For $\epsilon > 0.5$, the coarse solution does not exist any more (cf. Fig. 6 (b)) and therefore even a very strong bias does not impose the $P = 2P_{\rm het}$ solution. In a small intermediate range of d, the short-time evolution is attracted towards an unstable three-drop solution with the period $P = 4P_{\rm het}$, as indicated by the thick dotted lines in Figure 15 (b) and (c). On a slightly longer timescale ($t \approx 20$), the evolving profile is repelled from the unstable solution and approaches a linearly stable solution (corresponding to the second lowest horizontal line in Fig. 15 (c) and to the lowest branch in Fig. 9 at $\epsilon = 0.3$).

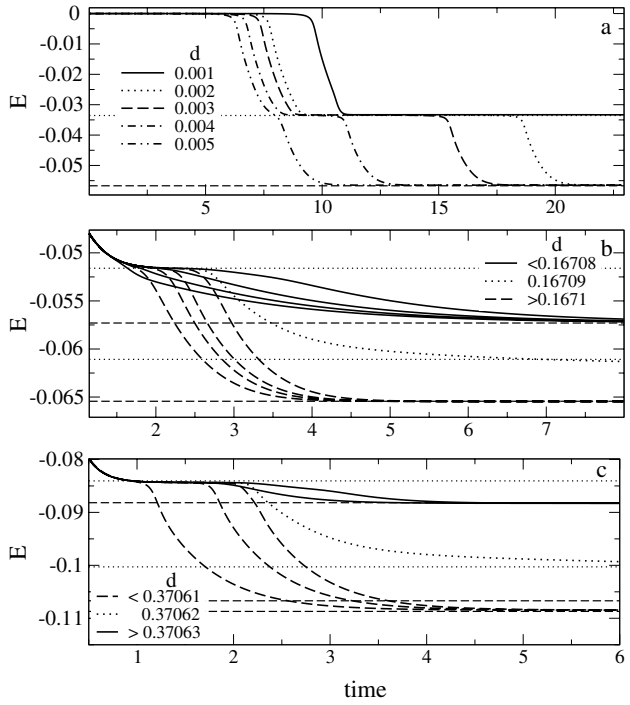

Fig. 15. Energy for the short-time evolution of a system of size $L = 4P_{\rm het}$ for (a) homogeneous substrate and heterogeneous substrates with (b) $\epsilon = 0.1$ and (c) $\epsilon = 0.3$. The initial condition is a flat film with a sinusoidal modulation of period $2P_{\rm het}$ and amplitude $d \times \bar{h}$ (as given in the legends). The remaining parameters are $\bar{h} = 2.5$, $P_{\rm het} = 50$, $G = 0.1$ and $a = 0.1$. In panels (b) and (c) solid lines approach the pinned solution ($P = P_{\rm het}$) and dashed lines the coarse solution with $P = 2P_{\rm het}$, *i.e.* only two drops remain in the system. The dotted lines approach unstable solutions with three drops. These solutions represent saddles in function space that first attract and subsequently repel the evolution. This implies that evolving solutions can come arbitrarily close to them during a transient time but will finally approach linearly stable solutions. Horizontal dotted (dashed) lines indicate the energy values of unstable (stable) periodic solutions as obtained from the bifurcation analysis in Section 2.2 corresponding to Figure 6 and Figure 9.

We found that in general the unstable solutions, *i.e.*, the saddle points in function space, may play a crucial role in the time evolution. If an evolving profile is attracted by one of these solutions it may remain a relatively long time close to it. Furthermore, the unstable solutions act as nucleation solutions between linearly stable solutions, *i.e.*, they define the energy barrier between them. So represent the uppermost horizontal lines in Figure 15 (b) and (c) the respective barriers between the pinned and the coarsed solutions and their special role can clearly be seen. Screening the initial conditions with a finer grid reveals more sub-ranges where (different) unstable solutions become important.

4 Transversal instability

So far we investigated two-dimensional drops, *i.e.* film thickness profiles that depend on only one spatial dimension. This is equivalent to a study of the longitudinal dynamics (in x-direction) of liquid ridges that are translationally invariant in the transversal direction y. Now we shall address the open question whether these ridges are stable with respect to perturbations in the transversal direction. Using linear stability analysis we compute the spectrum of eigenvalues (growth rates) β_i of small perturbations $\delta h_i(x) \exp(\beta_i t)(\exp(iky) + \text{c.c.})$ for a large set of transversal wave numbers k. The focus lies on two aspects: i) how is the transversal instability influenced by the heterogeneity and ii) what is the resulting three-dimensional morphology.

First, we consider the homogeneous substrate. There an individual liquid ridge is always transversally unstable with respect to a varicose mode that emerges from the zero-eigenvalue at $k = 0$ representing mass conservation. It is reminiscent of the Rayleigh instability known from liquid jets [69]. Figure 16 shows the cross-section of such a ridge in (a), the dispersion relations in (b), and the relevant eigenmodes $h_i(x)$ in (c). The second important eigenmode is a zigzag mode emerging from the zero-eigenvalue at $k = 0$ representing longitudinal translational invariance of the ridge. It is stable on the horizontal substrate, but becomes important for inclined substrates. For details on the homogeneous system see [50], where the transition towards an inclined substrate is discussed.

Having in mind the sinusoidal form of the heterogeneity one cannot decouple individual ridges because their width is of the order of their distance. The interaction of the ridges influences also the transversal stability of an array of ridges. Figure 17 shows the part of the eigenvalue spectrum with largest real part (black solid and dashed lines) for the transversal instabilities of a system of two neighbouring ridges. The corresponding eigenmodes and instability morphologies are depicted in Figure 18 with corresponding line styles. The varicose instability (solid lines) can take two forms: the instabilities of the two neighbour ridges may be transversally in-phase or anti-phase (Fig. 18 (a) and (b), respectively). The in-phase combination is a periodic continuation of the varicose instability of an individual ridge and has the same dispersion relation. The growth rate goes to zero as the wave number approaches zero and the eigenmode at $k = 0$ corresponds to the volume neutral mode. However, this is not the case for the anti-phase mode. For $k = 0$, it corresponds to the longitudinal coarsening mode by mass transfer between the two ridges as discussed in Section 2.2. Therefore for $k \to 0$ the growth rate does not approach zero but its maximal value (Fig. 17). For the zigzag mode (dashed lines, Figure 18 (c) and (d)), one finds that the in-phase mode is stable as for an individual ridge, but the anti-phase mode has a small band of unstable wave numbers around $k = 0$. It approaches for $k \to 0$ its largest growth rate corresponding to the one of the coarsening mode by translation. For the shown parameters the longitudinal coarsening by mass transfer is the dominant mode. Combinations of varicose and zigzag modes correspond to linear combinations of the already discussed modes. Studying larger arrays of more than two ridges allows for new combinations of in-phase

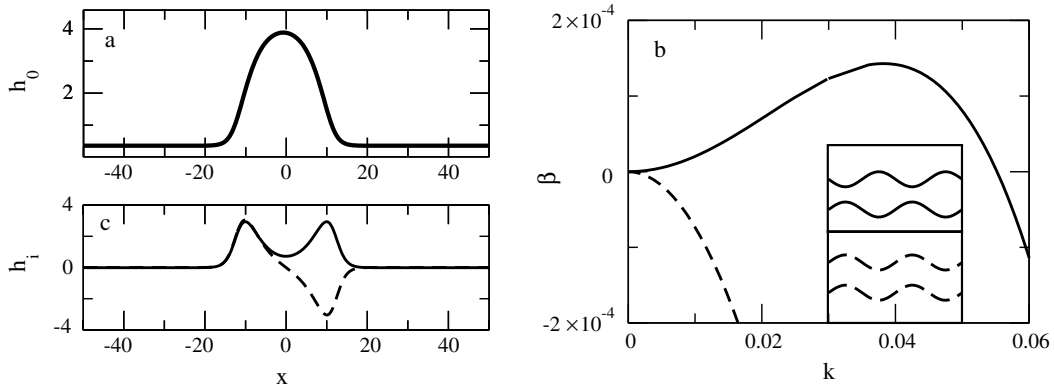

Fig. 16. Transverse stability of a ridge on a homogeneous substrate: (a) Ridge profile $h_0(x)$. (b) Dispersion relation $\beta(k)$ for the two transverse modes: the unstable varicose mode (solid) and the stable zigzag mode (dashed). The resulting structures are sketched in the inset. (c) The eigenmodes $h_i(x)$ corresponding to (b). The neutral modes obtained at $k = 0$ are very similar to the modes for the other k in (b). The parameters are $\bar{h} = 1.0$, $\epsilon = 0$, $L = P = 100$, $G = 0.1$, and $a = 0.1$.

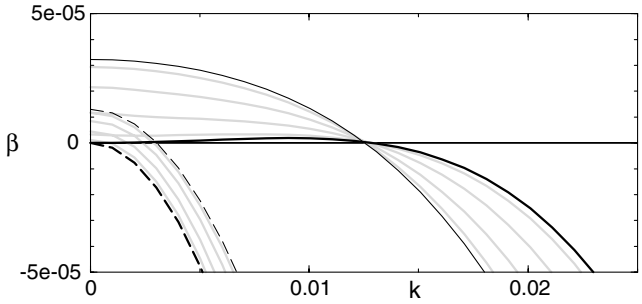

Fig. 17. Transversal instability of a ridge on a homogeneous substrate for a system of size $L = 2P_{\rm het}$ in x-direction. The four black lines show the growth rates for the transversal modes obtained from the four unique combinations of the two longitudinal eigenmodes. The linestyles correspond to the modes as represented in Figure 18. Grey lines show the growth rates for the additional modes in a system of size $L = 10P_{\rm het}$. Parameters are $\bar{h} = 2.5$, $\epsilon = 0$, $P_{\rm het} = 50$, $G = 0.1$, and $a = 0.1$.

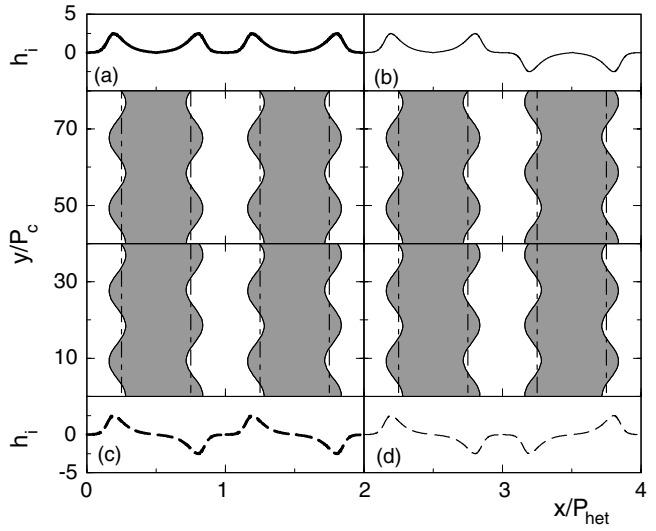

Fig. 18. Overview of the transversal instability modes. The translational and mass transfer neutral modes may be combined in four different ways to give the relevant transversal modes for a system containing two heterogeneous patches. The combinations are (a) two mass transfer modes of equal sign resulting in an in-phase varicose mode; (b) two mass transfer modes of opposite sign resulting in an anti-phase varicose mode; (c) two translational modes of equal sign resulting in an in-phase zigzag mode; and (d) two translational modes of opposite sign resulting in an anti-phase zigzag mode. The panels (a) to (d) show the respective eigenmodes h_i and a top view of the resulting morphology. Linestyles correspond to the ones of the dispersion relations in Figure 17.

and anti-phase neighbours. As discussed in Section 2.2 for longitudinal coarsening, the corresponding growth rates lie within the range given by the two-ridge system as indicated by the grey lines in Figure 17.

On heterogeneous substrates all growth rates decrease monotonously with increasing strength of the heterogeneity. This leads first to a shrinkage of the band of unstable wave numbers k and then to the complete stabilisation of the transversal instabilities. The unstable zigzag mode stabilises at smaller ϵ than the varicose modes. In general, we find the unstable eigenmode with largest wave number k to be the in-phase varicose mode. Figure 19 shows the growth rates for this mode at selected ϵ. Already at small ϵ the length scale of the transversal instability is much larger than the longitudinal period. For $\epsilon = 0.001$, for instance, the fastest growing mode has a wavelength of ≈ 1000 corresponding to twenty times $P_{\rm het}$. The critical heterogeneity where the band of unstable varicose modes vanishes is only slightly larger than the value where the longitudinal coarsening mode is stabilised. This is so for all ϵ (Fig. 8). Therefore, the exact boundary of linearly stable pinned ridges on a striped substrate is given by the critical heterogeneity for the transversal instability. However, for practical purposes it may be sufficient to calculate the critical ϵ for longitudinal coarsening.

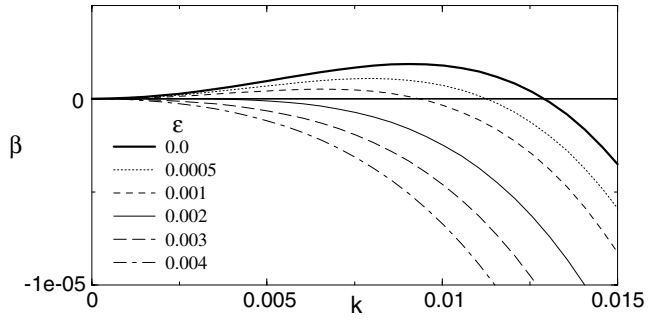

Fig. 19. The largest eigenvalues β *versus* wave number k of transversal perturbations for longitudinal system size $L = P_{\rm het}$. With increasing heterogeneity strength ϵ as given in the legend the range of unstable wave numbers becomes smaller and finally vanishes.

5 Conclusion

In the present work we have studied the pinning of a dewetting pattern by a substrate heterogeneity. Using a sinusoidally striped substrate, we have analysed the transition from coarsening via multistability of pinned and coarse morphologies to definite pinning with increasing strength of the heterogeneity. This characterises the pinning-coarsening transition as a first-order phase transition. By an extension towards transversal instabilities of liquid ridges we could show that these instabilities only slightly increase the strength of the heterogeneity necessary to image the substrate pattern.

The use of numerical bifurcation analysis yields not only the stationary periodic solutions but also the bifurcations between different types of such solutions. This provides a powerful tool to calculate morphological phase diagrams like Figure 8 without the need to probe the parameter space by full-scale numerical simulations in time. Here such simulations have rather been used to illustrate the behaviour predicted from the bifurcation analysis, especially in the range of multistability.

Furthermore, it was shown that upon increase of the system size, one finds an overproportional growth of the number of stationary solutions. Although most of these solutions are linearly unstable they nevertheless do influence the time evolution. This is due to the fact that they are saddle points in functional space, *i.e.* they attract the time evolution and then redirect it towards other saddles or stable solutions (as seen, for example, for $L = 4P_{\rm het}$ in Fig. 15). We predict that for intermediate heterogeneity the multitude of unstable solutions in large systems causes a strong sensitivity of the time evolution on the initial conditions. This is related to scenarios discussed for the transition to turbulence in Couette flow [70] and more recently for thin liquid films on a slightly inclined heated plane [13]. We conjecture that with an additional driving force, *i.e.*, for example, by inclining the substrate, these unstable solutions will cause a transition towards chaotic behaviour.

The linear stability analysis with respect to transversal instabilities showed the existence of four basic modes, namely in-phase and anti-phase varicose and zigzag modes. For the studied parameter values the in-phase varicose mode is the most important one for transversal modulation of the ridges, *i.e.* with the maximal growth rate for $k \neq 0$. However, it is overtaken by the coarsening mode that has its maximal growth rate for $k = 0$. For other parameter values this will be different as can already be seen from the results of Section 4. Recent three-dimensional computer simulations [41,63] seem to show both, in-phase and anti-phase morphologies depending on parameter values. A more comprehensive study of the transversal modes could be a worthwhile future undertaking.

Our investigations confirm for small heterogeneity the importance of the ratio between period of the heterogeneity and spinodal length scale of the corresponding homogeneous system. If the former is much smaller than the latter, patterns cannot be pinned to the heterogeneities. On the other hand, the smaller the spinodal length scale is the weaker the heterogeneity needs to be to pin the pattern. This observation offers the possibility to control templating by choosing an initial mass of fluid which yields a small spinodal length, *i.e.* the film thickness where the derivative of the disjoining pressure, $\partial M/\partial h$ is maximal. This observation confirms the results of direct numerical integrations of the film evolution equation for a substrate with strong stepwise heterogeneity with a qualitatively similar disjoining pressure [39]. Such piecewise homogeneous substrates may also be treated with the bifurcation analysis presented in this paper.

The comparison of the here presented results with results of the variational approach for striped substrates [35–37,43] yields two conclusions. i) Independently of the details of the model and the constraints, all the solution types found with the variational approach for the transversally invariant situation are represented in our model. On the one hand, this includes the "repelled" and "attracted" solutions of [36,37]. They correspond, respectively, to the upper and lower lines in Figure 6 (a). However, here the repelled solution is unstable. On the other hand, the homogeneous droplet pattern, inhomogeneous droplet pattern and the flat film denoted, respectively, (A), (B) and (C) in reference [35] correspond to some of the stable solutions of Figure 6 (b) and Figure 9. Furthermore, we found other linearly stable solutions beside these and so verify the conjecture of the existence of intermediate patterns, called (A_2) and (A_3) in reference [35] (corresponding to different coarse solutions). However, they do only exist in sub-ranges of the parameter space. ii) All results obtained here that refer to the actual evolution in time like growth rates and instability modes allow to obtain deeper insight in the ongoing processes. This is especially true for the transversal instability of a liquid ridge, where the spatial period of the fastest growing mode is generally not equal to the system size. The variational approach predicts the final stable state to consist of a ridge with a single bulge [43]. However, this final state may, for very small ridges, practically not be reached. There the transversal instability occurs with a finite wavelength (as calculated

here) followed by a very slow transversal coarsening (as can be seen in the simulations of references [38,41]).

The results derived here for dewetting on striped substrates carry over to the decomposition of binary mixtures in a narrow parallel slit between chemically striped plates or in a periodically modulated temperature field.

Moreover, we want to point out a similarity between the system studied here and the problem of fingering of a liquid front driven by gravity or a thermal gradient on homogeneous substrates [5,15] and heterogeneous substrates with stripes in the direction of the flow [71,72]. There, an initially straight liquid front develops into an array of advancing fingers. Far away from the liquid bulk, these fingers represent a system of parallel liquid ridges. Their profile orthogonal to the flow is independent of the coordinate in the direction of the flow. If the coordinate orthogonal to the flow is called x, these profiles are also solutions of equation (10) studied here. This applies to the homogeneous and the heterogeneous substrate. However, the important difference is the flow within the ridges that allows for different instability modes than the ones discussed here. This may lead to the observed selection of ridge distances on the homogeneous substrate. In the heterogeneous system, the transition between pinned fingers and coarse fingers, *i.e.* fingers over more than one stripe or not on each stripe, is also found on the inclined substrate [71,72]. However, the thresholds will be different due to the differing instability modes.

Altogether, the use of numerical bifurcation analysis proved an efficient tool and a useful supplement to direct numerical simulations of the film equations. It allows a fast determination of periodic film profiles possible on a striped substrate geometry for a wide range of parameters like heterogeneity length scale and strength. The described bifurcations and the related stability analysis provide a mathematically precise picture of the transition from coarsening to successful templating (pinning).

Appendix A. Numerical methods

Appendix A.1. Continuation

Finite-amplitude periodic solutions of equation (8) are calculated by numerical continuation techniques [44] after rewriting equation (10) as two ordinary differential equations of first order. Thereby the small-amplitude solutions equation (12) are used as starting solutions that are continued through the parameter space. One can vary the period of the heterogeneity, P_{het}, the mean film thickness, $\bar{h}$, the amplitude of the heterogeneity, ϵ, or the interaction parameters, G and a. At each of many subsequent steps in a single parameter, Newton's method is applied to the two ordinary differential equations discretized in space by typically 200 modes.

We fix, for example, P_{het}, $\bar{h}$, G and a, use periodic boundary conditions for h and $\partial_x h$ and look for solutions with different ϵ. Here the translational symmetry is already broken by the inhomogeneity and the extra boundary condition that is needed in the homogeneous case to select a unique solution [10] is not necessary. The resulting three boundary conditions and the integral condition that fixes the mean film thickness allow to determine the missing parameter C_1 for every ϵ.

Appendix A.2. Stability analysis

The longitudinal and transversal linear stability of the calculated stationary solutions $h_0(x)$ is obtained using the ansatz $h(x,y) = h_0(x) + \delta h_i(x)\exp(\beta_i t)(\exp(iky) + \text{c.c.})$ with $\delta \ll 1$ in equation (8). Linearisation in δ yields a eigenvalue problem for β_i and $h_i(x)$ with the transversal wave number k as an additional parameter. It is solved by discretisation of space by 128 Fourier modes. For the longitudinal stability k is set to zero. All eigenvalues β_i are real due to the variational structure of the problem. Positive (negative) values correspond to small perturbations of the form $h_i(x)$ that will exponentially grow (decay). The investigated solution is linearly stable if no β_i is positive. Instabilities and bifurcation points manifest themselves by zero crossings of the β_i.

Appendix A.3. Integration in time

Numerical integration of the time-dependent equation (8) for two-dimensional geometry, *i.e.* $h = h(x)$, is used to confirm the interpretation of the stationary solutions. We used a semi-implicit pseudo-spectral code and integrated equation (8) on a grid of 1024 mesh points. To avoid numerical instabilities for large amplitudes, we had to choose a small timestep of $\mathrm{d}t = 0.01$. The code was implemented on a Alpha Workstation XP1000. The simulation took a couple of minutes of CPU time to reach the pinned state. Coarsening can take several days depending on the details of the used noise. To get an impression of the influence of noise, we used additive white noise of amplitude η in equation (8). To avoid an enforcement of the numerical instability lurking at the length scale of the discretisation and to insure material conservation on the shortest length scale we use a "coarse" correlated noise, *i.e.* n neighbouring points are changed by an amount Δ and the next n points are changed by $-\Delta$. The choice $n = 3$ was used normally, but qualitatively identical results were obtained for $n = 4$ or $n = 5$.

References

1. A. Oron, S.H. Davis, S.G. Bankoff, Rev. Mod. Phys. **69**, 931 (1997).
2. M. Borgas, J. Grotberg, J. Fluid Mech. **193**, 151 (1988).
3. A. Sharma, E. Ruckenstein, J. Colloid Interface Sci. **106**, 12 (1985).
4. S.G. Bankoff, J. Heat Transf.-Trans. ASME **116**, 10 (1994).
5. H.E. Huppert, Nature **300**, 427 (1982).
6. V.S. Mitlin, J. Colloid Interface Sci. **156**, 491 (1993).
7. A. Sharma, R. Khanna, Phys. Rev. Lett. **81**, 3463 (1998).

8. A. Oron, Phys. Rev. Lett. **85**, 2108 (2000).
9. A.L. Bertozzi, G. Grün, T.P. Witelski, Nonlinearity **14**, 1569 (2001).
10. U. Thiele, M.G. Velarde, K. Neuffer, Y. Pomeau, Phys. Rev. E **64**, 031602 (2001).
11. A. Oron, P. Rosenau, J. Phys. II **2**, 131 (1992).
12. S.J. VanHook, M.F. Schatz, J.B. Swift, W.D. McCormick, H.L. Swinney, J. Fluid Mech. **345**, 45 (1997).
13. U. Thiele, E. Knobloch, submitted to Physica D (2002).
14. J.W. Cahn, J.W. Hilliard, J. Chem. Phys. **28**, 258 (1958).
15. M. Eres, L. Schwartz, R. Roy, Phys. Fluids **12**, 1278 (2000).
16. U. Thiele, M.G. Velarde, K. Neuffer, M. Bestehorn, Y. Pomeau, Phys. Rev. E **64**, 061601 (2001).
17. M. Bestehorn, K. Neuffer, Phys. Rev. Lett. **87**, 046101,1 (2001).
18. A.A. Golovin, A.A. Nepomnyashchy, S.H. Davis, M.A. Zaks, Phys. Rev. Lett. **86**, 1550 (2001).
19. G. Reiter, Phys. Rev. Lett. **68**, 75 (1992).
20. R. Seemann, S. Herminghaus, K. Jacobs, Phys. Rev. Lett. **86**, 5534 (2001).
21. C. Redon, F. Brochard-Wyart, F. Rondelez, Phys. Rev. Lett. **66**, 715 (1991).
22. R. Seemann, S. Herminghaus, K. Jacobs, Phys. Rev. Lett. **87**, 196101 (2001).
23. A. Sharma, G. Reiter, J. Colloid Interface Sci. **178**, 383 (1996).
24. G. Reiter, A. Sharma, Phys. Rev. Lett. **87**, 166103 (2001).
25. H.S. Kheshgi, L.E. Scriven, Chem. Eng. Sci. **46**, 519 (1991).
26. M. Mertig, U. Thiele, J. Bradt, D. Klemm, W. Pompe, Appl. Phys. A **66**, S565 (1998).
27. L. Rockford, Y. Liu, P. Mansky, T.P. Russell, M. Yoon, S.G.J. Mochrie, Phys. Rev. Lett. **82**, 2602 (1999).
28. H. Gau, S. Herminghaus, P. Lenz, R. Lipowsky, Science **283**, 46 (1999).
29. M. Gleiche, L.F. Chi, H. Fuchs, Nature **403**, 173 (2000).
30. A.M. Higgins, R.A.L. Jones, Nature **404**, 476 (2000).
31. P. Rehse, C. Wang, M. Hund, M. Geoghegan, R. Magerle, G. Krausch, Eur. Phys. J. E **4**, 69 (2001).
32. Y.N. Xia, D. Qin, Y.D. Yin, Curr. Opin. Colloid Interface Sci. **6**, 54 (2001).
33. A. Karim, J.F. Douglas, B.P. Lee, S.C. Glotzer, J.A. Rogers, R.J. Jackman, E.J. Amis, G.M. Whitesides, Phys. Rev. E **57**, R6273 (1998).
34. M. Mertig, R. Kirsch, W. Pompe, H. Engelhardt, Eur. Phys. J. D **9**, 45 (1999).
35. P. Lenz, R. Lipowsky, Phys. Rev. Lett. **80**, 1920 (1998).
36. C. Bauer, S. Dietrich, A. Parry, Europhys. Lett. **47**, 474 (1999).
37. C. Bauer, S. Dietrich, Phys. Rev. E **61**, 1664 (2000).
38. R. Konnur, K. Kargupta, A. Sharma, Phys. Rev. Lett. **84**, 931 (2000).
39. K. Kargupta, R. Konnur, A. Sharma, Langmuir **16**, 10243 (2000).
40. K. Kargupta, R. Konnur, A. Sharma, Langmuir **17**, 1294 (2001).
41. K. Kargupta, A. Sharma, Phys. Rev. Lett. **86**, 4536 (2001).
42. R. Lipowsky, Curr. Opin. Colloid Surf. Sci. **6**, 40 (2001).
43. M. Brinkmann, R. Lipowsky, J. Appl. Phys. **92**, 4296 (2002).
44. E.J. Doedel, A.R. Champneys, T. Fairgrieve, Y. Kuznetsov, B. Sandstede, X. Wang, *AUTO97: Continuation and Bifurcation Software for Ordinary Differential Equations* (Concordia University, Montreal, 1997).
45. E. Doedel, H.B. Keller, J.P. Kernevez, Int. J. Bifurcat. Chaos **1**, 493 (1991).
46. E. Doedel, H.B. Keller, J.P. Kernevez, Int. J. Bifurcat. Chaos **1**, 745 (1991).
47. U. Thiele, M.G. Velarde, K. Neuffer, Phys. Rev. Lett. **87**, 016104 (2001).
48. U. Thiele, K. Neuffer, Y. Pomeau, M.G. Velarde, Colloid Surf. A **206**, 135 (2002).
49. U. Thiele, K. Neuffer, M. Bestehorn, Y. Pomeau, M.G. Velarde, Colloid Surf. A **206**, 87 (2002).
50. U. Thiele, E. Knobloch, Phys. Fluids **15**, 892 (2003).
51. J. Skotheim, U. Thiele, B. Scheid, J. Fluid Mech. **475**, 1 (2003).
52. L. Brusch, H. Kühne, U. Thiele, M. Bär, Phys. Rev. E **66**, 011602 (2002).
53. P. Lenz, R. Lipowsky, Eur. Phys. J. E **1**, 249 (2000).
54. G.F. Teletzke, H.T. Davis, L.E. Scriven, Rev. Phys. Appl. **23**, 989 (1988).
55. R.J. Hunter, *Foundation of Colloid Science*, Vol. **1** (Clarendon Press, Oxford, 1992).
56. J.N. Israelachvili, *Intermolecular and Surface Forces* (Academic Press, London, 1992).
57. L.M. Pismen, Y. Pomeau, Phys. Rev. E **62**, 2480 (2000).
58. D.M. Anderson, G.B. McFadden, A.A. Wheeler, Annu. Rev. Fluid Mech. **30**, 139 (1998).
59. A. Sharma, A.T. Jameel, J. Colloid Interface Sci. **161**, 190 (1993).
60. A.T. Jammel, A. Sharma, J. Colloid Interface Sci. **164**, 416 (1994).
61. A. Sharma, R. Khanna, J. Chem. Phys. **110**, 4929 (1999).
62. A. Novick-Cohen, J. Stat. Phys. **38**, 707 (1985).
63. K. Kargupta, A. Sharma, Langmuir **18**, 1893 (2002).
64. R. Bausch, R. Blossey, M. Burschka, J. Phys. A **27**, 1405 (1994).
65. U. Thiele, M. Mertig, W. Pompe, Phys. Rev. Lett. **80**, 2869 (1998).
66. J. Bischof, D. Scherer, S. Herminghaus, P. Leiderer, Phys. Rev. Lett. **77**, 1536 (1996).
67. K. Kawasaki, T. Ohta, Physica A **116**, 573 (1982).
68. J. Guckenheimer, P. Holmes, *Nonlinear Oscillations, Dynamical Systems and Bifurkations of Vector Fields*, in *Applied Mathematical Sciences*, Vol. **42** (Springer-Verlag, Berlin, 1993).
69. S. Chandrasekhar, *Hydrodynamic and Hydromagnetic Stability* (Clarendon Press, Oxford, 1961).
70. A. Schmiegel, B. Eckhardt, Phys. Rev. Lett. **79**, 5250 (1997).
71. D.E. Kataoka, S.M. Troian, Nature **402**, 794 (1999).
72. L. Kondic, J.A. Diez, Phys. Rev. E **65**, 045301 (2002).